Block bond-order potential as a convergent moments-based method

T. Ozaki
Japan Advanced Institute of Science and Technology, Tatsunokuchi, Ishikawa 923-1292, Japan

M. Aoki
Department of Electrical Electronic Engineering, Gifu University, 1-1 Yanagido, Gifu 501-11, Japan

D. G. Pettifor
Department of Materials, University of Oxford, Parks Road, Oxford OX1 3PH, United Kingdom
(Received 20 August 1999)

The theory of a bond-order potential, which is based on the block Lanczos algorithm, is presented within an orthogonal tight-binding representation. The block scheme handles automatically the very different character of σ and π bonds by introducing block elements, which produces rapid convergence of the energies and forces within insulators, semiconductors, metals, and molecules. The method gives the first convergent results for vacancies in semiconductors using a moments-based method with a low number of moments. Our use of the Lanczos basis simplifies the calculations of the band energy and forces, which allows the application of the method to the molecular dynamics simulations of large systems. As an illustration of this convergent O(N) method we apply the block bond-order potential to the large-scale simulation of the deformation of a carbon nanotube.

I. INTRODUCTION

To understand mesoscale and macroscale phenomena from the atomistic level is an important subject in computer-aided materials modeling. This challenging study is not only intended as a realistic search for useful materials, but also for finding novel cooperative phenomena involving many atoms within large systems. Computer simulations of materials have inevitably promoted the development of efficient algorithms for dealing with long-time-scale phenomena. These methods have developed via two different approaches. The first, based on continuum mechanics, is a hybrid approach that combines continuum mechanics with atomistic simulations.[1,2] The second more directly applies the molecular dynamics (MD) simulation to large systems by reducing computational effort. The progress in these two approaches will enable us to bridge microscale and macroscale phenomena. In this paper we address the latter approach.

Atomistic simulations should be founded on a quantum-mechanical model in order to simulate a wide range of materials within a single framework, since the electronic structure determines the energy and the forces on atoms. The local-density approximation (LDA) to density functional theory[3–5] and semiempirical methods such as the tight-binding (TB) approximation[6,7] reduce the complicated quantum many-body interaction in condensed matter to a single-electron problem. The resultant theory has been applied to a variety of problems in materials science. However, it exceeds the capacity of modern computers to treat large systems that include thousands of atoms, using widely known methods for solving the single-electron problem such as the conjugate-gradient method, since the computational effort scales as the third power of the system size.

Therefore, several efficient methods with linear scaling algorithms have been proposed during the last decade.[8–20] These O(N) methods can be roughly divided into two categories: variational methods and moments-based methods. The former are the density matrix (DM) methods[19,20] and the localized orbital (LO) methods,[16–18] which lead to linear scaling algorithms from the localization of the density matrix and the Wannier functions, respectively. The latter include the bond-order potential (BOP) method[8–12] and the Fermi operator expansion (FOE) method,[13,14] which are intrinsically linear in the scaling of the computational effort because the enegy and forces are expanded in a finite moment expansion. Several applications of these variational methods have already been performed for large systems, which have shown the power of these O(N) methods.[21–23] However, several problems remain in these O(N) methods.

First, it is well known that the variational O(N) methods produce large errors in the energy of metallic systems with these long-range correlations in the density matrix.[24] In these cases there is no justification for cutting the matrix elements off at short distances in the density matrix. Unfortunately, if the cutoff distance is increased to decrease the error in the energy, then the calculation effort increases significantly.

Second, it is well documented that within moments-based methods, the vacancy in diamond or silicon cannot be described within a low number of moments (about 20).[24,25] A very large number of moments (about 200) is needed to reproduce the correct vacancy formation energy.[26] In the BOP method the forces become exact as the bond orders converge to the exact values. This implies that the forces are not consistent with the total energy if the recursion is terminated at a finite number of levels. In the other moments-based methods, such as the FOE method[13,14] and the global density of states method,[12,27] the exact forces can be calculated. However, these methods are also unable to reproduce the vacancy formation energy within a low number of moments.[24]

Any robust O(N) method should satisfy the following cri-

teria. First, the method should give accurate energies for a wide range of materials (insulators, semiconductors, metals, and molecules) with minimum computational effort. Second, the Hellmann-Feynman forces should be consistent with the total energy at any useful level of approximation. Third, the algorithm should be suitable for parallel computation.

Our goal is to establish the BOP method as an O(N) method that satisfies these three criteria. In Secs. II and III, we present the theory of the block BOP[10] within the orthogonal TB representation. We stress that the introduction of block elements into the BOP formalism improves remarkably the accuracy of the energy and forces. In Sec. IV we analyze the vacancy formation energy of diamond carbon in terms of the bond order and discuss the reason why the block BOP gives accurate energies in covalent materials with a low number of moments. In the remainder of this paper the deformation of a single-wall carbon nanotube is used to demonstrate the applicability of the method to large-scale atomistic simulations.

II. THEORY

A. Tight binding

We develop the block BOP within the two-center orthogonal TB representation.[7,28] It will be assumed that the basis set is an orthonormal set of atomiclike orbitals $|i\alpha\rangle$, where i is a site index and α an orbital index. The Hamiltonian can be represented by the matrix $H_{i\alpha,j\beta}=\langle i\alpha|\hat{H}|j\beta\rangle$. The on-site elements of the matrix are written as $\epsilon_{i\alpha}$. The cohesive energy, assuming that the electrons are at a finite temperature T, is the sum of bond, promotion, and repulsive energies:

$$E_{\rm coh}=E_{\rm bond}+E_{\rm prom}+E_{\rm rep}, \tag{1}$$

where the repulsive energy is given by the sum of pair potentials or embedded potentials that are usually determined so that the TB model reproduces equilibrium structures and elastic constants. The bond energy is the attractive contribution that leads to cohesion. There are two different but equivalent expressions that describe the bond energy. The first gives the bond energy in terms of the *on-site* density of states as follows:

$$E_{\rm bond}=2\sum_{i\alpha}\int (E-\epsilon_{i\alpha})n_{i\alpha}(E)f\left(\frac{E-\mu}{k_BT}\right)dE, \tag{2}$$

where $n_{i\alpha}(E)$ is the density of states projected onto orbital $|i\alpha\rangle$, and the function $f(x)=1/[1+\exp(x)]$ is the Fermi function. The second gives the bond energy explicitly in terms of the individual *intersite* bond energies as follows:

$$E_{\rm bond}=\frac{1}{2}\sum_{i\alpha\neq j\beta}(2\Theta_{i\alpha,j\beta}H_{j\beta,i\alpha}), \tag{3}$$

where $\Theta_{i\alpha,j\beta}$ is the bond order between orbitals $|i\alpha\rangle$ and $|j\beta\rangle$, and the expression in parentheses represents the corresponding bond energy associated with orbitals $|i\alpha\rangle$ and $|j\beta\rangle$. This allows us to interpret the bonding and structure of molecules and solids from a chemical point of view.[29] It should be noted that the bond order is not pairwise but is determined by the particular arrangement and connectivity of the atoms adjacent to the two atoms forming the bond. In the block BOP representation the two different expressions Eqs. (2) and (3) for the bond energy are exactly identical at any level of approximation. The proof will be given in a later subsection. The promotion energy is defined by

$$E_{\rm prom}=\sum_{i\alpha}(\epsilon_{i\alpha}N_{i\alpha}-\epsilon^0_{i\alpha}N^0_{i\alpha}), \tag{4}$$

where $N_{i\alpha}$ and $N^0_{i\alpha}$ are the number of electrons in $|i\alpha\rangle$ in the condensed and free atomic systems, respectively. The promotion energy is repulsive due to the excitation of electrons from their free atomic ground state as the atoms are brought together. Therefore, the cohesive energy of a system is determined by the balance between the attractive bond energy and the repulsive pairwise/embedding and promotion energies. The bond and promotion energies can be repartitioned into the band and atomic energies:

$$\begin{aligned}E_{\rm bond}+E_{\rm prom}&=\sum_{i\alpha\neq j\beta}\Theta_{i\alpha,j\beta}H_{j\beta,i\alpha}+\sum_{i\alpha}(\epsilon_{i\alpha}N_{i\alpha}-\epsilon^0_{i\alpha}N^0_{i\alpha})\\&=\sum_{i\alpha,j\beta}\Theta_{i\alpha,j\beta}H_{j\beta,i\alpha}-\sum_{i\alpha}\epsilon^0_{i\alpha}N^0_{i\alpha}\\&=E_{\rm band}-E_{\rm atoms}.\end{aligned} \tag{5}$$

$E_{\rm band}$ is equal to the energy that is defined by integrating $\Sigma_{i\alpha}En_{i\alpha}(E)$ up to the Fermi level.

In the TB model the single-particle eigenfunctions are expanded in a basis set that is an orthonormal set of real atomiclike orbitals: $|i\alpha\rangle$,

$$|\phi\rangle=\sum_{i\alpha}C^{(\phi)}_{i\alpha}|i\alpha\rangle, \tag{6}$$

where the expansion coefficients are defined by $C^{(\phi)}_{i\alpha}\equiv\langle i\alpha|\phi\rangle$. $C^{(\phi)}_{i\alpha}$ is always real because of real atomic orbitals and Hamiltonian. Then the bond orders may be defined in terms of the expansion coefficients as follows:

$$\Theta_{i\alpha,j\beta}=2\sum_{\phi}C^{(\phi)}_{j\beta}C^{(\phi)}_{i\alpha}f\left(\frac{\epsilon^{(\phi)}-\mu}{k_BT}\right), \tag{7}$$

where the factor 2 accounts for spin degeneracy. $\epsilon^{(\phi)}$ is the eigenvalue corresponding to an eigenstate $|\phi\rangle$.

The force on atom k is obtained by differentiating Eq. (1) with respect to atomic positions:

$$\begin{aligned}\mathbf{F}_k&=-\frac{\partial E_{\rm coh}}{\partial\mathbf{r}_k}\\&=-\sum_{i\alpha,j\beta}\left(\frac{\partial\Theta_{i\alpha,j\beta}}{\partial\mathbf{r}_k}H_{j\beta,i\alpha}+\Theta_{i\alpha,j\beta}\frac{\partial H_{j\beta,i\alpha}}{\partial\mathbf{r}_k}\right)-\frac{\partial E_{\rm rep}}{\partial\mathbf{r}_k}.\end{aligned} \tag{8}$$

The first term of Eq. (8) is identically zero in insulators at zero electronic temperature so that

$$\mathbf{F}_k=-\sum_{i\alpha,j\beta}\Theta_{i\alpha,j\beta}\frac{\partial H_{j\beta,i\alpha}}{\partial\mathbf{r}_k}-\frac{\partial E_{\rm rep}}{\partial\mathbf{r}_k}, \tag{9}$$

where the first term of Eq. (9) is the Hellmann-Feynman force. If the bond orders are approximate values, then the

sum of the derivatives of the bond orders with respect to atomic positions will not be zero, so that Eq. (8) gives the exact force that is consistent with the total energy in insulators at zero temperature. In insulators and metals at nonzero temperature, on the other hand, the sum is not alway zero. However, in the block BOP representation the forces are given by Eq. (9), since it is very difficult to evaluate the derivatives of the bond orders. Hence, the forces calculated by block BOP become exact as the bond orders converge to the exact values. In Sec. II the compatibility between the force and the energy will be discussed from numerical tests using constant energy molecular dynamics simulations.

Although the forces are not consistent with the total energy in the usual BOP methods, it is possible to evaluate the exact forces at any level of approximating by the other momentsbased method, the global density of states method.[27] However, the use of the global moments, which are introduced to decrease the computational effort, leads to a reduced rate of convergence of the energy as a function of the number of moments. In the Appendix of this paper we present a novel method to evaluate the exact forces.

B. Block bond-order potential

The local density of states and bond orders can be related to the one-particle Green's functions. The one-particle Green's function operator is defined by

$$\hat{G}(Z)=(Z-\hat{H})^{-1}=\sum_{\phi}\frac{|\phi\rangle\langle\phi|}{Z-\epsilon^{(\phi)}}. \tag{10}$$

Then the imaginary part of the diagonal elements of the Green's function matrix give the local density of states:

$$\begin{aligned}\mathrm{Im}\,G_{i\alpha,i\alpha}(E+\mathrm{i}0^{+})&=\sum_{\phi}\frac{-0^{+}\langle i\alpha|\phi\rangle\langle\phi|i\alpha\rangle}{(E-\epsilon^{(\phi)})^{2}+(0^{+})^{2}}\\&=-\pi\sum_{\phi}\,(C_{i\alpha}^{(\phi)})^{2}\delta(E-\epsilon^{(\phi)})\\&=-\pi n_{i\alpha}(E).\end{aligned}$$

Therefore

$$n_{i\alpha}(E)=-\frac{1}{\pi}\mathrm{Im}\,G_{i\alpha,i\alpha}(E+\mathrm{i}0^{+}), \tag{11}$$

where $G_{i\alpha,i\alpha}(Z)=\langle i\alpha|\hat{G}(Z)|i\alpha\rangle$, 0^{+} represents a positive infinitesimal, and $\delta(x)$ is the delta function. The imaginary part of the off-diagonal elements of the Green's function matrix has the following relation to the expansion coefficients of the single-particle eigenfunctions:

$$\mathrm{Im}\,G_{i\alpha,j\beta}(E+\mathrm{i}0^{+})=-\pi\sum_{\phi}\,C_{j\beta}^{(\phi)}C_{i\alpha}^{(\phi)}\delta(E-\epsilon^{(\phi)}). \tag{12}$$

Multiplying the both sides of Eq. (12) by the Fermi function and integrating with respect to the energy, we obtain the following useful expression for the bond order:

$$\begin{aligned}\mathrm{Im}\int G_{i\alpha,j\beta}(E+\mathrm{i}0^{+})f\left(\frac{E-\mu}{k_BT}\right)dE&=-\pi\sum_{\phi}\,C_{j\beta}^{(\phi)}C_{i\alpha}^{(\phi)}\int\delta(E-\epsilon^{(\phi)})f\left(\frac{E-\mu}{k_BT}\right)dE\\&=-\pi\sum_{\phi}\,C_{j\beta}^{(\phi)}C_{i\alpha}^{(\phi)}f\left(\frac{\epsilon^{(\phi)}-\mu}{k_BT}\right)\\&=-\frac{\pi}{2}\Theta_{i\alpha,j\beta}.\end{aligned}$$

Therefore

$$\Theta_{i\alpha,j\beta}=-\frac{2}{\pi}\mathrm{Im}\int G_{i\alpha,j\beta}(E+\mathrm{i}0^{+})f\left(\frac{E-\mu}{k_BT}\right)dE. \tag{13}$$

The evaluations of the bond energy Eqs. (2) and (3) require calculating the local density of states and bond orders. We obtain the local density of states and bond orders from the Green's function through Eqs. (11) and (13). The diagonal elements of the Green's function matrix can be calculated in a numerically stable way by the recursion method.[30,31] Block BOP is a general recursion method for evaluating efficiently both the diagonal and off-diagonal elements of the Green's function matrix by the recursion method. The first step of the recursion method is to tridiagonalize the Hamiltonian using the Lanczos algorithm.[32] In the block BOP we introduce the *block* Lanczos algorithm with the starting state as a single site containing all the valence orbitals rather than the usual *scalar* Lanczos algorithm with a single starting orbital.[10] However, the application of the conventional block algorithm[33,34] to finite systems such as molecules introduces a numerical instability, since the terminal number of recursion levels of the π bond are different from that of the σ bond in the recursive algorithm. Therefore, we modify the conventional block Lanczos algorithm. A series of procedures for the modified block Lanczos algorithm can be carried out as follows:

$$|U_0)=(|i1\rangle,|i2\rangle,\ldots,|iM_i\rangle), \tag{14}$$

$$\underline{A}_n=(U_n|\hat{H}|U_n), \tag{15}$$

$$|r_n)=\hat{H}|U_n)-|U_{n-1})^{t}\underline{B}_n-|U_n)\underline{A}_n, \tag{16}$$

$$(\underline{B}_{n+1})^{2}=(r_n|r_n), \tag{17}$$

$$(\underline{\lambda}_n)^{2}={}^{t}\underline{V}_n(\underline{B}_{n+1})^{2}\underline{V}_n, \tag{18}$$

$$\underline{B}_{n+1}=\underline{\lambda}_n{}^{t}\underline{V}_n, \tag{19}$$

$$(\underline{B}_{n+1})^{-1}=\underline{V}_n\underline{\lambda}_n^{-1}, \tag{20}$$

$$|U_{n+1})=|r_n)(\underline{B}_{n+1})^{-1}. \tag{21}$$

$\underline{A}_n$ and $\underline{B}_n$ are recursion block coefficients $M_i\times M_i$ in size, where M_i is the number of atomic orbitals on the starting atom i, and the underline indicates that the element is a block.

The states $|U_n)=(|L_{n1}\rangle,|L_{n2}\rangle,\ldots,|L_{nM_i}\rangle)$ represent the Lanczos basis, and are orthonormal and block-tridiagonalize

the Hamiltonian. The modified algorithm gives different expressions for the block elements $\underline{B}_{n+1}$ and these inverses compared with the conventional algorithm. The block elements in the conventional block Lanczos algorithm are defined by

$$\underline{B}_{n+1}=\underline{V}_n\underline{\lambda}_n{}^t\underline{V}_n, \tag{22}$$

$$(\underline{B}_{n+1})^{-1}=\underline{V}_n\underline{\lambda}_n^{-1t}\underline{V}_n. \tag{23}$$

The failure in the conventional algorithm can be illustrated by a carbon trimer with a linear chain structure along the x axis. If the block Lanczos algorithm is applied with the central atom in the trimer as the starting state, then the p_y and p_z orbitals span two independent subspaces. Thus, the recursive algorithm finishes after only one iteration for the Lanczos vectors concerned with the p_y and p_z orbitals. This gives two zero eigenvalues in the four eigenvalues of the block element $(\underline{B}_2)^2$. Then one cannot evaluate the inverse of $\underline{B}_2$ using Eq. (23). Therefore, defining $\underline{B}_2$ and its inverse by the modified equations (19) and (20), respectively, and assuming that the diagonal elements of $\underline{\lambda}_1^{-1}$ corresponding to the zero eigenvalues are zero, we have

$$\underline{B}_2(\underline{B}_2)^{-1}=\begin{pmatrix}1&&&\\&1&&\\&&0&\\&&&0\end{pmatrix}, \tag{24}$$

$$(U_2|U_2)=\begin{pmatrix}1&&&\\&1&&\\&&0&\\&&&0\end{pmatrix}. \tag{25}$$

$|U_2)$ is reduced to the state with two vectors, while the starting state $|U_0)$ is constructed by the four vectors, which permits us to iterate once more with the recursive algorithm. The conventional block Lanczos algorithm does not satisfy both Eqs. (24) and (25), since the block elements $\underline{B}_2$ and the inverse are obtained from the unitary transformations of $\underline{\lambda}_1$ and the inverse, respectively. Therefore, the conventional algorithm terminates at this recursion level even though the Lanczos vectors for the σ orbital can still hop. This reduction of the state avoids the numerically instabilities for the case of small eigenvalues of $(\underline{B}_{n+1})^2$, even when the eigenvalues are not zero.

Application of the block Lanczos algorithm defines an orthonormal basis set called the Lanczos vector or basis. The Lanczos vectors reflect the neighboring atomic arrangement of the starting site. In Fig. 1 we show the Lanczos vectors on an s-valent square lattice. The Lanczos vectors spread gradually from the central atom as the number of recursion levels increases. Thus, we now expand a one-electron eigenstate using the Lanczos vectors

$$|\phi\rangle=\sum_{n\nu} D_{n\nu}^{(\phi)}|L_{n\nu}\rangle, \tag{26}$$

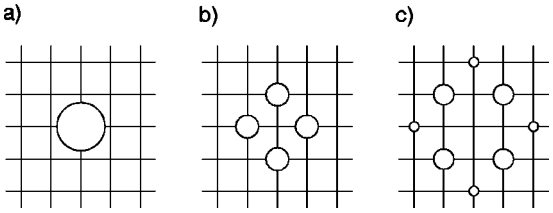

FIG. 1. The Lanczos vectors on the s-valent square lattice. (a), (b), and (c) are an initial state $|L_0\rangle$, $|L_1\rangle$, and $|L_2\rangle$, respectively. The diameter of the circles is proportional to the magnitude of the expansion coefficient in the Lanczos vector.

where $D_{n\nu}^{(\phi)}\equiv\langle L_{n\nu}|\phi\rangle$. Then the representation based on the atomic basis can be transformed into that of the Lanczos basis set by the matrix U such that

$$T^L={}^tUTU, \tag{27}$$

where U is defined by $\langle i\alpha|L_{n\nu}\rangle$, and T can be the Hamiltonian H, the derivative of Hamiltonian with respect to atomic position $\partial H/\partial\mathbf{r}_i$, the bond order Θ, or the Green's function $G(Z)$ matrix. The index L indicates the representation based on the Lanczos basis. Equation (27) is a pseudounitary transformation, and the matrix U becomes unitary when the number of the recursion levels is infinity in infinite systems. If the block Lanczos algorithm is started through Eq. (14) with the atomic orbitals on atom i as the starting state, then considering Eq. (27) and the orthonormality of the Lanczos basis, we can relate the bond orders in the Lanczos basis representation to the bond orders based on the atomic basis by the following simple relation:

$$\underline{\Theta}_{ij}=\sum_n \underline{\Theta}_{0n}^L{}^t\underline{U}_{nj}, \tag{28}$$

where $\underline{\Theta}_{ij}$ and $\underline{\Theta}_{0n}^L$ are the block elements of the bond orders for the atoms i and j and the states $|U_0)$ and $|U_n)$, respectively. For example, $\underline{\Theta}_{ij}$ signifies

$$\underline{\Theta}_{ij}=\begin{pmatrix}\Theta_{i1,j1}&\Theta_{i1,j2}&\cdots&\Theta_{i1,jM_j}\\\Theta_{i2,j1}&\Theta_{i2,j2}&\cdots&\Theta_{i2,jM_j}\\\cdots&\cdots&\cdots&\cdots\\\Theta_{iM_i,j1}&\Theta_{iM_i,j2}&\cdots&\Theta_{iM_i,jM_j}\end{pmatrix}, \tag{29}$$

where M_i and M_j are the numbers of atomic orbitals including atoms i and j, respectively. In Eq. (28) ${}^t\underline{U}_{nj}$, which is the (n,j) block element of the matrix ${}^tU$, is defined by

$${}^t\underline{U}_{nj}=\begin{pmatrix}\langle L_{n1}|j1\rangle&\langle L_{n1}|j2\rangle&\cdots&\langle L_{n1}|jM_j\rangle\\\langle L_{n2}|j1\rangle&\langle L_{n2}|j2\rangle&\cdots&\langle L_{n2}|jM_j\rangle\\\cdots&\cdots&\cdots&\cdots\\\langle L_{nM_i}|j1\rangle&\langle L_{nM_i}|j2\rangle&\cdots&\langle L_{nM_i}|jM_j\rangle\end{pmatrix}. \tag{30}$$

The simple relation Eq. (28) allows us to evaluate the bond order in terms of the Lanczos basis representation. We have only to calculate the zeroth block line, which is the bond orders between the starting atom and the Lanczos vectors surrounding the atom, of the bond-order matrix. In the block

BOP the bond orders are evaluated in the Lanczos basis representation, and then we get the bond orders based on the atomic basis from Eq. (28).

It is essential to start the block Lanczos algorithm with a single site as in Eq. (14). Although it is possible to derive an analogous transformation to Eq. (28) using the usual scalar Lanczos algorithm, the bond energy of the system depends on the rotation of the system.[34] Thus, the use of the scalar algorithm is not appropriate, since the bond energy should be invariant to the rotation of the system. We could also start the recursion with a cluster containing a neighbor shell of atoms instead of a single site.[33] However, this choice is unsuitable because it is highly computationally intensive.

In the Lanczos representation the Hamiltonian is block-tridiagonalized:

$$(U_m|\hat{H}|U_n)=\begin{cases}\underline{A}_n & \text{if } m=n,\\ {}^t\underline{B}_n & \text{if } m=n-1,\\ \underline{B}_{n+1} & \text{if } m=n+1,\\ \underline{0} & \text{otherwise.}\end{cases} \tag{31}$$

The block element $\underline{G}_{00}(Z)=(U_0|\hat{G}|U_0)$ can be written explicitly by the form of the multiple inverse, since the Green's function matrix $G(Z)$ is the inverse of the matrix $(ZI-H)$. Appling repeatedly the partitioning method,[35,36] which is a method for calculating the inverse of matrices, to the matrix $(ZI-H)$, we get

$$\underline{G}^L_{00}(Z)=[Z\underline{I}-\underline{A}_0-{}^t\underline{B}_1[Z\underline{I}-\underline{A}_1-{}^t\underline{B}_2[\cdots]^{-1}\underline{B}_2]^{-1}\underline{B}_1]^{-1}. \tag{32}$$

$\underline{G}^L_{00}(Z)$ is equal to the block element $\underline{G}_{ii}(Z)$ based on the atomic basis, since we have started the block Lanczos algorithm with Eq. (14). Therefore, the local density of states can be evaluated from the diagonal elements by Eq. (11). Also the trace of $\underline{G}^L_{00}(Z)$ gives the local density of states on atom i.

Moreover, by taking account of the block-tridiagonalized Hamiltonian and the identity $(ZI-H)G(Z)=I$ in the Lanczos basis representation, the off-diagonal elements of the Green's function matrix $\underline{G}^L_{0n}$ may be obtained from the following recurrence relation:

$$\underline{G}^L_{0n}(Z)=[\underline{G}^L_{0n-1}(Z)(Z\underline{I}-\underline{A}_{n-1}) -\underline{G}^L_{0n-2}(Z){}^t\underline{B}_{n-1}-\delta_{1n}\underline{I}](\underline{B}_n)^{-1}, \tag{33}$$

where δ is the Kronecker's delta, and $\underline{G}_{0-1}(Z)$ and ${}^t\underline{B}_0$ are $\underline{0}$. All the off-diagonal block elements $\underline{G}^L_{0n}(Z)$ are related to the diagonal block element $\underline{G}^L_{00}(Z)$. Once $\underline{G}^L_{00}(Z)$ has been obtained, the off-diagonal block elements are easily evaluated from the above recursive relation. The simplicity of evaluating the off-diagonal block elements is an important advantage of the Lanczos basis representation. The block elements of the Green's function matrix have the same relation to the bond orders based on the Lanczos basis as that of the atomic basis representation:

$$\underline{\Theta}^L_{0n}=-\frac{2}{\pi}\,\mathrm{Im}\int \underline{G}^L_{0n}(E+\mathrm{i}0^+)f\left(\frac{E-\mu}{k_BT}\right)dE. \tag{34}$$

In case the bond orders are evaluated by Eqs. (28) and (34), we can prove that the two different expressions Eqs. (2) and (3) for the bond energy are identical at any level of approximation. Consider the trace of $G(Z)(ZI-H)$. Transforming the trace of the atomic basis representation into that of the Lanczos basis using Eq. (27), and making use of the identity $G(Z)(ZI-H)=I$ in the Lanczos basis representation, we see that the trace is a constant:

$$\begin{aligned}&\mathrm{tr}\{G(Z)(ZI-H)\}\\ &=\sum_i \mathrm{tr}\{Z\underline{G}_{ii}(Z)\}-\sum_{ij}\mathrm{tr}\{\underline{G}_{ij}(Z)\underline{H}_{ji}\}\\ &=\sum_i \mathrm{tr}\{Z\underline{G}^{L^{(i)}}_{00}(Z)\}-\sum_{in}\mathrm{tr}\{\underline{G}^{L^{(i)}}_{0n}(Z)\underline{H}^{L^{(i)}}_{n0}\}\\ &=\sum_i \mathrm{tr}(\underline{I}^{(i)}),\end{aligned} \tag{35}$$

where $\underline{I}_i$ is a unit matrix with $M_i\times M_i$ in size. The index $L^{(i)}$ indicates the representation based on the Lanczos basis with the starting state on atom i. Considering the imaginary parts of the trace, we have

$$\mathrm{Im}\sum_{i\alpha} ZG_{i\alpha,i\alpha}(Z)=\mathrm{Im}\sum_{i\alpha,j\beta}G_{i\alpha,j\beta}(Z)H_{j\beta,i\alpha}. \tag{36}$$

We see that the two expression for the bond energy give the same energy, since the Green's functions can be related to the local density of states and bond orders through Eqs. (11) and (13), respectively. The block BOP, thus, provides the equivalence of the two expressions for the bond energy in a natural way, whereas in the usual BOP the Green's functions need a carefully chosen truncator in order to satisfy the sum rule.[9]

C. Moment description

The moments of the local density of states allow us to link the behavior of the electronic structure to the local topology about the given site.[11,12,29] We now discuss the relation between the block recursion matrices and the moments of the density of states. From Eq. (10) for $|Z|\to\infty$, the diagonal element $\underline{G}^L_{00}(Z)$ can be rewritten as follows:

$$\begin{aligned}\underline{G}^L_{00}(Z)&=\sum_\phi \frac{(U_0|\phi\rangle\langle\phi|U_0)}{Z-\epsilon^{(\phi)}}\\ &=\sum_\phi \underline{d}^{(\phi)}_{00}\left(\sum_{p=0}^{\infty}\frac{(\epsilon^{(\phi)})^p}{Z^{p+1}}\right)=\sum_{p=0}^{\infty}\frac{\underline{\mu}^{(p)}_{00}}{Z^{p+1}},\end{aligned} \tag{37}$$

where

$$\underline{d}^{(\phi)}_{00}=\begin{pmatrix} D^{(\phi)}_{i1}D^{(\phi)}_{i1} & D^{(\phi)}_{i2}D^{(\phi)}_{i1} & \cdots & D^{(\phi)}_{ip}D^{(\phi)}_{i1}\\ D^{(\phi)}_{i1}D^{(\phi)}_{i2} & D^{(\phi)}_{i2}D^{(\phi)}_{i2} & \cdots & D^{(\phi)}_{ip}D^{(\phi)}_{i2}\\ \cdots & \cdots & \cdots & \cdots\\ D^{(\phi)}_{i1}D^{(\phi)}_{ip} & D^{(\phi)}_{i2}D^{(\phi)}_{ip} & \cdots & D^{(\phi)}_{ip}D^{(\phi)}_{ip}\end{pmatrix}, \tag{38}$$

$$\underline{\mu}_{00}^{(p)}=\sum_{\phi}\underline{d}_{00}^{(\phi)}(\epsilon^{(\phi)})^{p}, \tag{39}$$

and $\underline{\mu}_{00}^{(p)}$ is the block element of the pth moment for the atom i, the diagonal elements of which give the pth moments of the projected density of states $n_{i\alpha}(E)$. Thus, Eq. (37) is the moment expansion of the Green's function $\underline{G}_{00}^{L}(Z)$. Also the pth block moment can be evaluated explicitly as the expectation value of the pth power of the Hamiltonian in terms of the block elements $\underline{A}_n$, $\underline{B}_n$:

$$\begin{aligned}\underline{\mu}_{00}^{(p)}&=(U_0|\hat{H}^{p}|U_0)\\&=\sum_{m_1\cdots m_{p-1}}(U_0|\hat{H}|U_{m_1})\\&\quad\times(U_{m_1}|\hat{H}|U_{m_2})\cdots(U_{m_{p-1}}|\hat{H}|U_0).\end{aligned} \tag{40}$$

The first few block moments are

$$\begin{aligned}\underline{\mu}_{00}^{(0)}&=\underline{I},\\\underline{\mu}_{00}^{(1)}&=\underline{A}_0,\\\underline{\mu}_{00}^{(2)}&=(\underline{A}_0)^2+{}^{t}\underline{B}_1\underline{B}_1.\end{aligned} \tag{41}$$

From Eq. (40) we see that the pth moment is the sum over all self-returning paths of length p. The first moment corresponds to a hop on a single site, the second to nearest neighbors and back, and so on. Thus, the atomic connectivity can be related directly to the electronic structure through the description of the Green's function by the moments.

Multiplying both sides of Eq. (37) by $(E+0^{+})^{r}$, and integrating with respect to the energy E we get the following relation:

$$-\frac{1}{\pi}\,\mathrm{Im}\int_{-\infty}^{\infty}E^{r}\underline{G}_{00}^{L}(E+0^{+})dE=\underline{\mu}_{00}^{(r)}. \tag{42}$$

This relation means that the imaginary part of the moment of the block-diagonal element in the Green's function matrix is equal to the moment of the Hamiltonian.

Let us define the orthogonal block polynomials $\underline{P}_n(x)$:

$$x\underline{P}_n(x)=\underline{P}_n(x)\underline{A}_n+\underline{P}_{n-1}(x){}^{t}\underline{B}_n+\underline{P}_{n+1}(x)\underline{B}_{n+1}, \tag{43}$$

where $\underline{P}_{-1}(x)$ and $\underline{P}_0(x)$ are the zero matrix $\underline{0}$ and the unit matrix $\underline{I}$ with $M_i\times M_i$ in size. By using the block polynomials the recursion block elements $\underline{A}_n$ and $\underline{B}_n$ can be expanded with the moments:

$$\begin{aligned}\underline{A}_n&=(U_n|H|U_n)\\&={}^{t}\underline{P}_n(\hat{H})(U_0|\hat{H}|U_0)\underline{P}_n(\hat{H})\\&=\sum_{m}^{2n+1}\underline{a}_m\underline{\mu}_{00}^{(m)}\underline{a}'_m,\end{aligned} \tag{44}$$

$$\begin{aligned}\underline{B}_n&=(U_n|H|U_{n-1})\\&={}^{t}\underline{P}_n(\hat{H})(U_0|\hat{H}|U_0)\underline{P}_{n-1}(\hat{H})\\&=\sum_{m}^{2n}\underline{b}_m\underline{\mu}_{00}^{(m)}\underline{b}'_m.\end{aligned} \tag{45}$$

In the derivations of Eqs. (44) and (45) we have assumed the substitution. $|U_0)\hat{H}\rightarrow\hat{H}|U_0)$ and $\hat{H}(U_0|\rightarrow(U_0|\hat{H}$. The block coefficients $\underline{a}_m$, $\underline{a}'_m$, $\underline{b}_m$, and $\underline{b}'_m$ are given by the recursion block elements. For example $\underline{A}_1$ and $\underline{B}_1$ can be written as follows:

$$\underline{A}_1=({}^{t}\underline{B}_1)^{-1}\{\underline{\mu}_{00}^{(3)}-\underline{A}_0\underline{\mu}_{00}^{(2)}-\underline{\mu}_{00}^{(2)}\underline{A}_0+\underline{A}_0\underline{\mu}_{00}^{(1)}\underline{A}_0\}(\underline{B}_1)^{-1}, \tag{46}$$

$$\underline{B}_1=({}^{t}\underline{B}_1)^{-1}\{\underline{\mu}_{00}^{(2)}-\underline{A}_0\underline{\mu}_{00}^{(1)}\}. \tag{47}$$

In case the recursion in the block Lanczos algorithm is terminated at the qth level, the diagonal block element of the Green's function matrix can be expanded with the $(2q+1)$th moments, because it is constructed by the multiple inverse with the recursion block elements $\underline{A}_n(n=0-q)$, $\underline{B}_n(n=1-q)$ given by the qth recursion. As shown in Eqs. (44) and (45), the recursion block elements are expanded in terms of the moments. Thus, $\underline{G}_{00}^{L}$ contains the zeroth to $(2q+1)$th moments. This implies that up to the $(2q+1)$th moment is included in the sum of the moment expansion Eq. (37), and Eq. (42) satisfies for $r\leqslant 2q+1$.

To obtain the moments for the off-diagonal elements of the Green's function matrix, multiplying both sides in Eq. (33) by $(E+0^{+})^{r}$ and integrating with respect to the energy E, we have

$$\begin{aligned}&\mathrm{Im}\int_{-\infty}^{\infty}E^{r}\underline{G}_{0n}^{L}(E+0^{+})dE\\&\quad=\sum_{m=0}^{n}\left(\mathrm{Im}\int_{-\infty}^{\infty}E^{r+m}\underline{G}_{00}^{L}(E+0^{+})dE\right)\underline{c}_m,\end{aligned} \tag{48}$$

where the block coefficients $\underline{c}_m$ can be written in terms of the recursion block elements. As mentioned above the right side of Eq. (48) is equal to the moment of the Hamiltonian for $r+m\leqslant 2q+1$, so that the left side gives the exact moment $\underline{\mu}_{0n}^{(r)}$ for $r\leqslant 2q+1-n$. This means that the off-diagonal elements of the Green's function matrix can be expanded with up to the $(2q+1-n)$th moment, which results in the expansion of the bond order $\underline{\Theta}_{0n}^{L}$ by up to the $(2q+1-n)$th moment. Moreover, we can relate the bond orders in the atomic basis representation to the moments through the transformation Eq. (28). In the right side of Eq. (28) the bond order $\underline{\Theta}_{0q}^{L}$ for $n=q$ determines the maximum order of the moments for the bond orders based on the atomic basis. So we see that the bond orders in the atomic basis representation can be expanded with the moments for $r\leqslant q+1$. Thus, in the block BOP the off-diagonal elements of the Green's function matrix can be constructed with the moments for $r\leqslant q+1$, while the diagonal elements have the information of the moments for $r\leqslant 2q+1$. This could imply the difference in the convergence properties of the bond energy and the forces. After a

simple consideration it is estimated that the rate of the convergence of the force is about half as fast as that of the bond energy in terms of recursion levels. However, it should be noted that the contribution of $\underline{\Theta}^L_{0n}$ to $\underline{\Theta}_{ij}$ decreases as the recursion level n increases, since the Lanczos vectors, which hop repeatedly in the atomic connectivity, have their weight away from the starting atom as the recursion level n increases. Thus, the bond orders in the atomic basis representation do not have all the moments of the higher order more than the $(q+1)$th, but can include the higher moments through the $\underline{G}^L_{0n}$ for $n<q$. In this case, whereas the inexact moments for $r \leqslant 2q+1-n$ are included in the bond order in the atomic basis representation, the error can be negligible, since the bond orders $\underline{\Theta}^L_{0n}$ become small as the recursion level n increases. So it is stressed that the higher moments can be included in the bond order based on the atomic basis through the Green's function $\underline{G}^L_{0n}$ for small recursion levels n. Therefore, it is expected that the forces should be comparable to the bond energy in terms of the convergence rate. In Sec. III we will discuss this point again numerically.

D. Details on implementation

The technical details to implement the block BOP are given in this subsection. For an infinite system, there could be an infinite number of levels in the multiple inverse of the diagonal Green's function. It is often the case, however, that the exact values can be replaced by estimated values after a certain number of levels, without reducing the accuracy significantly. The simplest approximation is to take $\underline{A}_n=\underline{A}_\infty$, $\underline{B}_n=\underline{B}_\infty$ for $n>n_t$, where n_t is the number of exact levels, and $\underline{A}_\infty$ and $\underline{B}_\infty$ are constant block elements. This approximation is reasonable from the observation that the scalar elements in both $\underline{A}_n$ and $\underline{B}_n$ converge to constant values or oscillate around constant values as n tends to infinity.[34] We have only to replace the level for $n=n_t+1$ in the multiple inverse with the terminator, since the constant terms can be summed exactly. The terminator can be written by a closed form including itself as follows:

$$\underline{T}(Z)=[Z\underline{I}-\underline{A}_\infty-{}^t\underline{B}_\infty\underline{T}(Z)\underline{B}_\infty]^{-1}. \tag{49}$$

However, this is still a difficult set of equations to solve, so to simplify matters we assume that the off-diagonal elements of $\underline{T}(Z)$ are zero and all the diagonal elements are the same, since the differences between the diagonal elements of $\underline{A}_n$ and $\underline{B}_n$ become small as the number of the recursion levels increases, respectively. Then the identical diagonal element $t(Z)$ of $\underline{T}(Z)$ is written as the square-root terminator:

$$t(Z)=[Z-a-b^2t(Z)]^{-1}=\frac{1}{b}\left[\frac{Z-a}{2b}-i\sqrt{1-\left(\frac{Z-a}{2b}\right)^2}\right], \tag{50}$$

where a and b^2 are given by the means of the diagonal elements of $\underline{A}_{n_t}$ and $\underline{B}^2_{n_t}$, respectively. Thus, we see that the effect of the terminator is to smear out the sharp states with energy a into semielliptical bands. The degree of smearing is given by b.

There are two ways to conserve charge neutrality in the system: local charge neutrality[7] (LCN) or the total charge neutrality[10] (TCN). Within LCN the on-site energies are varied (keeping the splitting between on-site s and p energy levels fixed) in order to conserve the number of electrons on each atom. If the excess charge on site i is $Q_i=Z_i-\Sigma_\alpha N_{i\alpha}$, where Z_i is the effective core charge, then the on-site energies can be shifted using the response function $X_i=\Sigma_\alpha X_{i\alpha}$ for atom i as follows:

$$\epsilon'_{i\alpha}=\epsilon_{i\alpha}-\lambda\frac{Q_i}{X_i}, \tag{51}$$

where λ is a parameter to accelerate the convergence, and generally is 1.0. The response function projected on an atomic orbital $i\alpha$ is given by

$$X_{i\alpha}=\frac{2}{\pi}\,\mathrm{Im}\int[G_{i\alpha,i\alpha}(E+i0^+)]^2 f\left(\frac{E-\mu}{k_BT}\right)dE. \tag{52}$$

Usually no more than three or four iterations are required to achieve the convergence so that the absolute value of Q/atom is below 10^{-5}, since $X_{i\alpha}\simeq\partial N_{i\alpha}/\partial\epsilon_{i\alpha}$. The assumption of LCN has the advantage that the Madelung energy contribution is zero, so that the TB model need not take this into account in its expression for the energy. Also LCN is suitable for parallel computation, since the calculations of the bond energy and the forces of each atom are perfectly independent within the assumption. However, LCN brings an inefficiency in terms of computational effort, since LCN requires the Lanczos algorithm to be implemented again, after the charge neutralities of all the atoms has been achieved, since the recursion block elements are varied by the shift of the on-site energies. Thus, the block Lanczos algorithm and the shift of the on-site energies must be repeated until self-consistency is accomplished. This self-consistency requires typically 20 iterations. This discourages us from applying LCN in the molecular dynamics simulations. On the other hand, we can conserve the total number of electrons in the system by a shift of the chemical potential in terms of TCN. If the excess charge of the system is $Q=\Sigma_i Q_i$, then a good approximation of the chemical potential is given by

$$\mu'=\mu+\lambda\frac{Q}{X}, \tag{53}$$

where $X=\Sigma_i X_i$. The convergence is achieved after only three or four iterations. The TCN assumption, corresponding to the microcanonical distribution, has a physically appropriate meaning, which is consistent with the usual electronic structure calculations by diagonalization. Moreover, within TCN we need not repeat the Lanczos algorithm, since the recursion block elements are not varied by the shift of the chemical potential. Thus, TCN has a considerable advantage in terms of computational effort. The TCN condition reduces the separability of individual atoms in the calculations of the band energy and forces, and complicates slightly the ability to structure the program code in parallel form. However, the evaluation and integration of the Green's function, which are time-consuming steps, are performed separately. Therefore, we use the TCN constraint to conserve the total number of electrons.

It is required to integrate the Green's functions with the Fermi function in order to evaluate the bond energy, bond

orders, and response functions. The integration can be carried out in the complex plane by summing up an infinite series over the modified Matsubara poles.[11,12,37] The general form can be given as follows:

$$\mathrm{Im}\int A(E+i0^{+})f(x)dE=-\frac{2\pi}{\beta}\,\mathrm{Re}\left[\lim_{P\to\infty}\sum_{p=0}^{P-1}z_pA(E_p)\right], \tag{54}$$

with

$$E_p=\mu+\frac{2P}{\beta}(z_p-1),\quad z_p=\exp\left(\frac{i\pi(2p+1)}{2P}\right), \tag{55}$$

where $A(x)$ is an arbitrary function defined in the complex plane, and $\beta=1/k_BT$. Also E_p are the poles of the approximated Fermi function in the complex plane. This modified Matsubara summation converges rapidly with about 40 complex poles ($P\simeq 40$) with a high electron temperature ($k_BT>0.1$ eV), although many poles are needed to achieve the convergence with a lower electron temperature. In the case of systems with a gap between the valence and conduction bands, we need to pay attention to the evaluation of the chemical potential, since the response functions in the gap become zero as k_BT tends to 0, so that it is difficult to estimate the chemical potential under a low electron temperature using Eq. (53). This can be solved by smearing the density of states under a high electron temperature. Thus, it is required to evaluate the response functions at high electronic temperatures in order to obtain stable MD simulations.

We now estimate the time dependence within the block BOP. The total system is divided into finite clusters centered on individual atoms in order to evaluate the energy and force of each atom. The size of the finite cluster is not determined by the size of the total system, but by the system and the condition of the MD simulation. Therefore, the computational effort is proportional to the number of atoms N_{atom}, so that the number of computational operations can be written as cN_{atom}, where c is a proportionality constant. The scaling of the constant c can be estimated as a function of the numbers of recursion level q, atoms within a finite cluster n_c, and orbitals on an atom M. For simplicity it is assumed that the system consists of only one type of element with M orbitals. In the block Lanczos algorithm the time-consuming step is the product of the Hamiltonian matrix and the vector, so that the count of operations in the block Lanczos algorithm is nearly proportional to qn_c^2M. At the next step, the inverses and recursive calculations are required to evaluate the diagonal and off-diagonal elements of the Green's function matrix, respectively, and their integrations are performed as the sum of the residues for the poles in the complex plane, so that the count of operations for the evaluations is almost proportional to qPM^3. Thus, the proportionality constant c can be estimated as $c_Lqn_c^2M+c_GqPM^3$, where c_L and c_G are prefactors of the count of operations for the block Lanczos algorithm and the the evaluation of the bond orders, respectively. The prefactors depend on the computer, the system, and the criterion of charge neutrality. For example, for the case of a three-hop cluster, 10 recursion levels, and 40 complex poles for diamond carbon, the calculation time of the block Lanczos algorithm is comparable to that in evaluating and integrating the Green's functions.

In the remainder of this section the procedure for implementing the block BOP is enumerated.

(I) *The partition of the system*. The hopping range of each atom is determined by terminating the system. There are two ways to terminate the system. One of them is the physical truncation that the terminated cluster contains atoms within a sphere with a certain cutoff radius. The physical truncation can bring inaccurate properties into the convergence of the energies, since atoms that have no bonding to other atoms can be included in the neighborhood of the cluster surface. Moreover, in MD simulations the energies can jump discontinuously when an atom moves in or out of the surface of the sphere. The more stable way is logical truncation. The cluster of size n is here defined by all neighbors that can be reached by n hops. Provided the cutoff distance for the hopping integral is identical to that defining the connectivity of the bonding, the energies are continuous as a function of time in MD simulations. Therefore, it is desirable to truncate the system logically in terms of accuracy.

(II) *The block Lanczos algorithm*. The Hamiltonians for the individual terminated clusters are constructed. For these small cluster Hamiltonians the block Lanczos algorithm Eqs. (14)–(21) is applied.

(III) *The evaluations and integrations of the Green's functions*. In the Lanczos basis representation the diagonal and the off-diagonal elements of the Green's functions are evaluated using Eqs. (32) and (33), respectively, and then their integrations are performed via the modified Matsubara summation with Eq. (54).

(IV) *The transformation into the atomic basis representation*. The bond orders based on the Lanczos basis are transformed into those in the atomic basis representation using Eq. (28).

(V) *The bond energy and forces*. From Eqs. (3) and (9) the bond energy and forces are evaluated, respectively.

III. CONVERGENCE PROPERTIES

O(N) methods with linear scaling algorithms are approximate approaches compared to the exact diagonalization for dealing with large-scale systems, so that the realization of the O(N) algorithms is accompanied by decreases in computational accuracy in exchange for computational efficiency. Therefore, O(N) methods should only be applied to atomistic simulations once their accuracy and efficiency has been tested.

In the block BOP three approximations are introduced to reduce the computational effort: the number of moments, or recursion levels, the size of the cluster of atoms over which the hops are made, and a finite number of poles in the modified Matsubara summation, which gives accurately integration of Green's functions with the Fermi function within a small number of poles. The finite approximations for the number of levels and the size of the cluster can lead to the errors in the energies and forces. Thus, we now investigate the block BOP through several test calculations in terms of its accuracy and efficiency. In order to ascertain applicable bounds for a wide range of materials, the energy and force convergence are examined for an insulator (carbon[38] in the

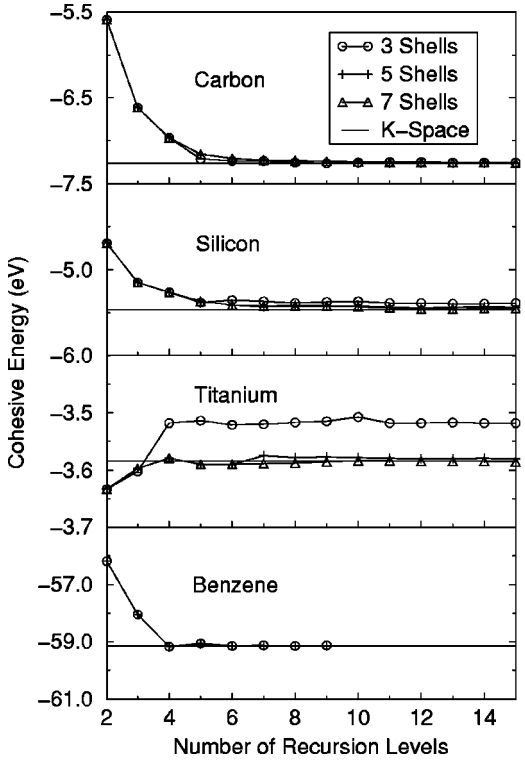

FIG. 2. The cohesive energy for carbon in the diamond structure, silicon in the diamond structure, hcp titanium, and benzene as a function of number of recursion levels for three-, five-, and seven-shell clusters, calculated using a square-root terminator, and $k_BT = 0.1$ eV.

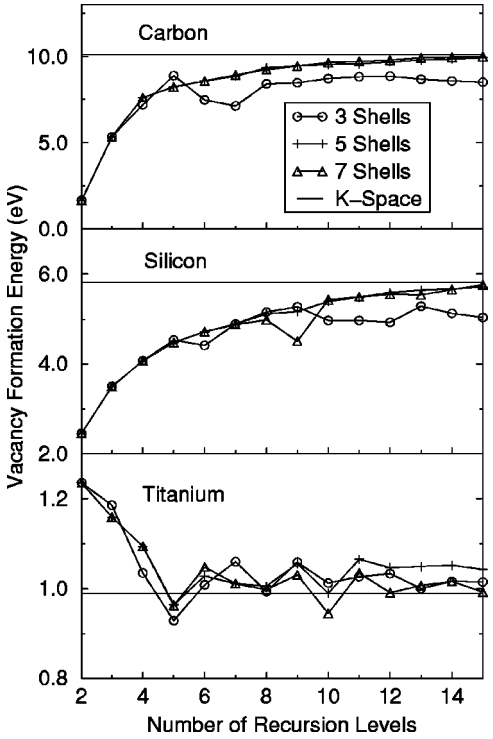

FIG. 3. The vacancy formation energy for carbon in the diamond structure, silicon in the diamond structure, and hcp titanium for three-, five-, and seven-shell clusters as a function of number of recursion levels, calculated using a square-root terminator, a total charge neutrality, and $k_BT = 0.1$ eV.

diamond structure), a semiconductor (silicon[39]), a metal (titanium, described by a canonical *d*-band model), and a molecule (benzene[40]) as functions of the number of recursion levels and the size of cluster. In all the test calculations, we have chosen the same value (40 poles) as the number of poles in the modified Matsubara summation. The 40 poles is enough to achieve convergence in carbon, silicon, titanium, and benzene materials in case of $k_BT = 0.1$ eV used in all the numerical tests.[12] Moreover, in terms of the computational efficiency the block BOP is compared with *k*-space calculations in computational time. Also as a test of the quality of the forces, we perform a constant energy molecular dynamics (CEMD) simulation of carbon.

Figure 2 shows the cohesive energy per atom for carbon in the diamond structure, silicon in the diamond structure, hcp titanium, and benzene. The cohesive energies were calculated using 2–15 recursion levels (a numerical instability often appears for >20 recursion levels) for three, five, and seven shell clusters by the logical truncation method, where the three-, five-, and seven-shell clusters for the diamond structure include 41, 147, and 363 atoms, respectively, and these clusters for the hcp structure contain 153, 587, and 1483 atoms, respectively. The cohesive energies for carbon and silicon converge rapidly to the results of *k*-space calculations. The errors for carbon and silicon are only 1% at six recursion levels. Thus, we see that up to the 13th moment corresponding to six recursion levels determine the cohesive energies. The contribution of the higher-order moments is unimportant, since the convergence properties are almost identical for three-, five-, and seven-shell clusters. The cohesive energy for silicon converges more slowly compared with that of carbon in the rate of convergence for the size of cluster. This suggests that a semiconductor such as silicon requires a higher moment than an insulator such as carbon for good convergence of the cohesive energy. The cohesive energy for the metallic hcp titanium converges very quickly in terms of the number of recursion levels. For the five and seven shell clusters the cohesive energy converges fully to the *k*-space result, while the convergence value for the three-shell cluster is in error by 2% from the *k*-space result. For benzene the convergence is achieved with a very small cluster (two shells). The error at four recursion levels is only 0.1%. We see that the block BOP can evaluate accurately the cohesive energy for a molecule with a sparse structure like benzene, which has both localized σ bonds and delocalized π bonds.

The calculation of the vacancy formation energy is a severe test to distinguish the accuracy of different O(N) methods, since it is a criterion that tests the precision with which the dangling bonds caused by the vacancy are handled by O(N) method. In practice, the usual moment-based O(N) methods fail to reproduce the vacancy formation energy of carbon in the diamond structure even when dozens of moments are included.[24,25] The computational error at 30 moments is still about 20% compared to the *k*-space result. In Fig. 3 we show the vacancy formation energy for carbon in the diamond structure, silicon in the diamond structure, and hcp titanium. These are calculated as the difference between the energy for a bulk unit cell (of 64, 64, or 32 atoms, respectively) with a single atom removed, and the perfect bulk cell energy scaled to 63, 63, or 31 atoms. The results are for

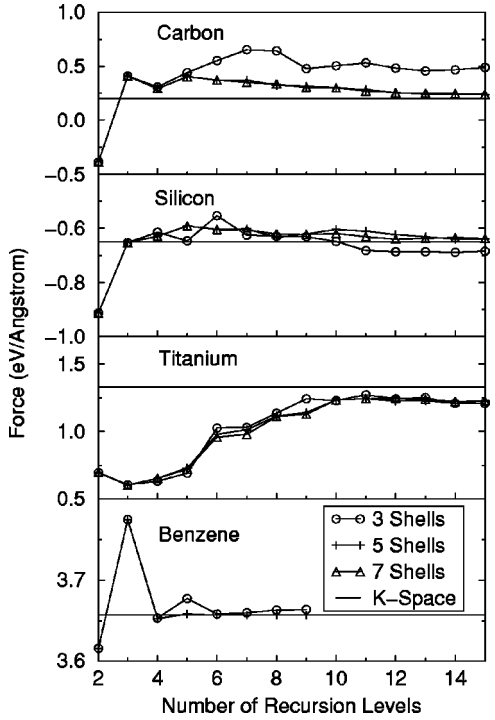

FIG. 4. The z component of the force on an atom on the carbon (001) surface, silicon (001) surface, titanium (001) surface, and on a hydrogen atom in benzene for three-, five-, and seven-shell clusters as a function of number of recursion levels, calculated using a square-root terminator, total charge neutrality, and $k_BT=0.1$ eV.

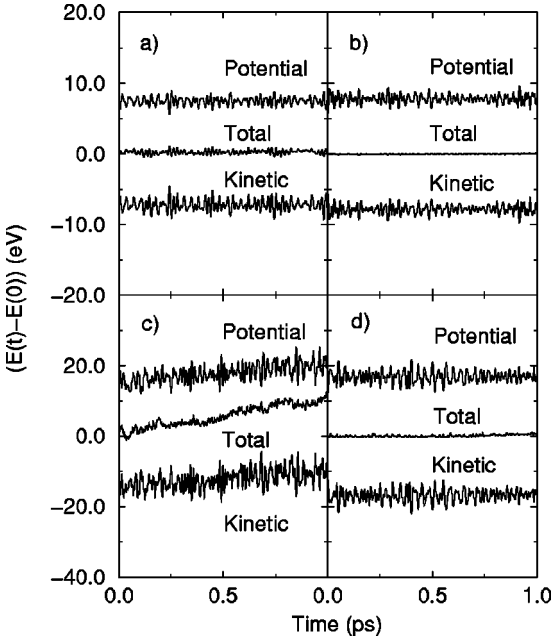

FIG. 5. The potential, kinetic, and total energies as a function of time for molecular dynamics simulations of carbon using a three-hop logically truncated cluster, a square-root terminator, total charge neutrality, and $k_BT=0.1$ eV. In panels (a) and (b) the results are for five and ten recursion levels at 1000 K, respectively, whereas in panels (c) and (d) they are for five and ten recursion levels at 5000 K, respectively. The time step is 0.5 fs.

an unrelaxed vacancy. The convergence properties for carbon and silicon are almost identical. The vacancy formation energy in the five- and seven-shell clusters converges smoothly toward the k-space results, while in the three-shell cluster the converged values for carbon and silicon are 15%, and 13% underestimated, respectively. In the seven-shell cluster at 15 recursion levels the errors for carbon and silicon are only 1%. Thus, we see that the block BOP gives an accurate vacancy formation energy for strongly covalent materials such as carbon and silicon with the use of about 30 block moments. This remarkable result suggests that the block BOP accurately describes dangling bonds in comparison with the usual moment-based methods. In Sec. IV we will discuss the advantages inherent in the block BOP by analyzing the vacancy formation energy in terms of different bond-order contributions. For titanium the vacancy formation energy converges to the k-space result equally within the three-, five-, and seven-shell clusters. The error for the three-shell cluster at five recursion levels is about 6%. The vacancy formation energy oscillates with respect to the number of recursion levels due to the long-range value of the density matrix (see Fig. 2 of Ref. 23). The oscillations are damped by imposing LCN instead of TCN to conserve the number of electrons.

The accuracy of the forces is investigated from two different perspectives. The first is the accuracy when compared to the exact k-space result; the second is the degree of correspondence between the numerical and analytic Hellmann-Feynman forces. In order to perform reliable MD simulations the two criteria should be satisfied. In Fig. 4 we show the z component of the force on an atom in the bulk-terminated (001) surface of carbon, silicon, and hcp titanium and the force on a hydrogen atom on benzene. For carbon the force of the three-shell cluster overestimates by about 130% in comparison with the k-space result, although the error in the Hellmann-Feynman term is only 1%. The forces of the five- and seven-shell clusters converge smoothly toward the k-space result. The rate of convergence in silicon is much better than that of carbon. Even the three-shell cluster shows a converged value that differs by only 5% from the k-space result. The three-, five-, and seven-shell clusters of Ti show similar convergence properties of the forces, the converged value being underestimated by about 8% compared with the k-space result. For benzene the force converges rapidly with small cluster size. As discussed in Sec. II the bond orders can be expanded using the lower-order moments compared with the density of states in the block BOP. It can be estimated that the forces should converge more slowly at the k-space results than the bond energies, since the forces on the atoms are evaluated using the bond orders. However, these numerical results for the forces show that the convergence rate of the force is comparable to that of the bond energy. This means that the sum of Eq. (28) converges rapidly as the number of the recursion levels increases because of the diffusion of the Lanczos vectors.

As a test of the consistency between the total energy and the forces, CEMD simulations have been performed for carbon. If the forces are equal to the derivative of the total energy with respect to atomic positions, the total energy of the system is conserved. Thus, the CEMD simulation is a criterion to investigate the consistency of forces. In Fig. 5 we show the energy for carbon at 1000 and 5000 K as a function of time using five and ten recursion levels. The initial struc-

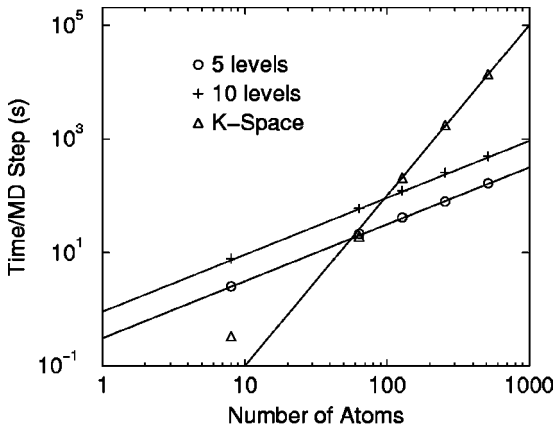

FIG. 6. The time to perform the energy and the force evaluation for carbon in the diamond structure as a function of number of atoms in the cell for the block BOP, calculated using a three-hop logically truncated cluster, and *k* space. The calculations were performed on an IBM RS/6000 workstation.

ture is the diamond lattice, and the unit cell is fixed in volume and shape. When the initial temperature of the system is 1000 K, the atoms oscillate around the equilibrium positions. At five and ten recursion levels we see that the total energy is almost conserved. When the temperature is raised to 5000 K, the carbon in the diamond structure transforms into liquid carbon with mainly a threefold-coordinate structure. From Fig. 5 we see that the forces are of good quality at ten recursion levels, while the total energy at five recursion levels increases by about 10 eV during 1 ps, which corresponds to a temperature increase of 1800 K. These results indicate that the block BOP can give forces consistent with the total energy, provided the proper number of recursion levels is used, even for liquid materials such as carbon at a high temperature. On the other hand, in the variational DM method, although only the Hellmann-Feynman term survives formally as the derivatives of the band energy with respect to atomic coordinates, total energy of liquid silicon in the CEMD simulation exhibits a steady upward drift.[41]

To study the computational efficiency of the block BOP we carry out two benchmark tests: the comparison between the block BOP and the *k*-space calculation in computer time, and the relation between the computational error and the computer time. Figure 6 shows the time to evaluate the energy and forces for a cell containing carbon in the diamond structure as function of the number of atoms in the cell for the block BOP and *k*-space using a single *k*-point. The crossover point at which the block BOP becomes favorable is about 100 atoms.

Figures 7(a) and 7(b) show the relation between the error and the the time per atom to evaluate the energy and forces in the calculations of the vacancy formation energy of diamond carbon and hcp titanium, respectively. Here the increase in time corresponds to the increase of the number of recursion levels. We see that the block BOP can calculate the vacancy formation energy to high accuracy within almost the same computational time as the other moment-based results reported by Bowler *et al.*,[24] where the calculations were performed using the same computational facilities. We note that the block BOP has given a good convergent result of the vacancy formation energy in diamond carbon for the first

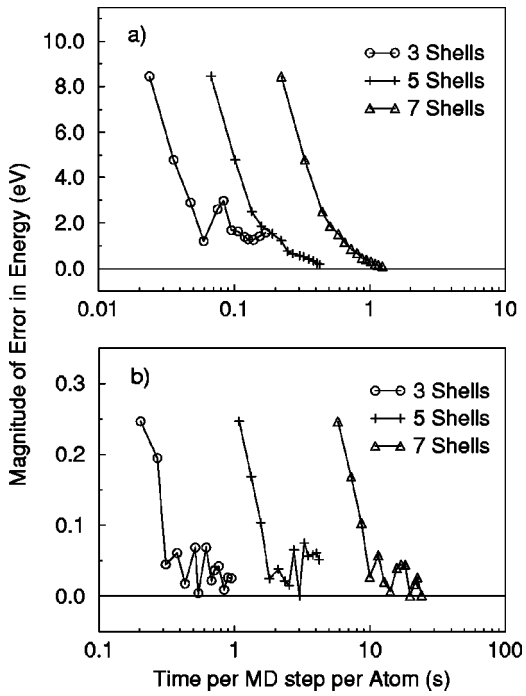

FIG. 7. The error in the (a) carbon and (b) titanium vacancy formation energies against the time taken per MD step per atom for three-, five-, and seven-shell clusters. The calculations were carried out with a square-root terminator, total charge neutrality, and $k_BT = 0.1$ eV on a HP9000/735 workstation.

time with a moments-based method, while the computational time to achieve this convergence is still ten times slower than that of the DM method. This work, therefore, still supports the conclusions of the study in Ref. 23 that the DMM is best for systems with energy gaps, but that moments-based methods such as BOP are best for metallic systems.

IV. ANALYSIS OF VACANCY FORMATION ENERGY

The block BOP can provide chemical insight into the nature of the bonding in molecules and solids in terms of the bond order. The bond order is a useful quantity indicating the strength of bonding between two atoms. In practice, it is well

TABLE I. Comparison of the original and the reduced TB method with respect to the predicted cohesive energies of carbon in the perfect diamond structure and the diamond unit cell including 64 atoms with a single atom removed. The calculations were performed with a logical truncation of a seven-shell cluster, 15 recursion levels, a square-root terminator, local charge neutrality, and $k_BT = 0.1$ eV.

	Perfect (eV/atom)	Vacancy (eV/atom)	Vacancy formation energy (eV)
Original			
k space	−7.251	−7.091	10.110
BOP	−7.249	−7.090	10.004
Reduced			
k space	−7.254	−7.098	9.860
BOP	−7.256	−7.100	9.783

known that the bond length is nearly proportional to the bond order for the π bonded hydrocarbons.[42]

In this section we analyze the vacancy formation energy of carbon in the diamond structure in terms of the bond order, and discuss the reason why the usual moment-based methods cannot reproduce the vacancy formation energy even with several dozens of moments.[24,25] The reduced TB model[43–46] is introduced in order to clarify the analysis of the vacancy formation energy in terms of the two scalar bond orders Θ_σ and Θ_π, respectively. In the reduced TB model the three independent bond integrals $h_{ss\sigma}$, $h_{pp\sigma}$, and $h_{sp\sigma}$ are reduced to the two independent variables h_σ and p_σ by assuming that $h_{sp\sigma}$ is the geometric mean of $|h_{ss\sigma}|$ and $h_{pp\sigma}$. This allows the σ bond energy between atoms i, and j to be written as the single quantities $h_\sigma(R_{ij})\Theta_\sigma^{ij}$ rather than the sum of three terms $h_{ss\sigma}\Theta_{ss\sigma}$, $2h_{sp\sigma}\Theta_{sp\sigma}$, and $h_{pp\sigma}\Theta_{pp\sigma}$, respectively. That is, we can write

$$E_{\rm bond}^{(ij)}=E_\sigma^{(ij)}+E_\pi^{(ij)} =-2h_\sigma^{(ij)}\Theta_\sigma^{(ij)}-4h_\pi^{(ij)}\Theta_\pi^{(ij)}, \tag{56}$$

where

$$h_\sigma=(1+p_\sigma)|h_{ss\sigma}|, \tag{57}$$

$$\Theta_\sigma=\frac{\Theta_{ss\sigma}+2\sqrt{p_\sigma}\Theta_{sp\sigma}+p_\sigma\Theta_{pp\sigma}}{1+p_\sigma},$$

with $p_\sigma=h_{pp\sigma}/|h_{ss\sigma}|$. All the hopping integrals and bond orders are defined as positive quantities. In addition, the cutoff distance in the hopping integrals and repulsive potential is reduced from 2.6 Å in the original TB fit[38] to 2.5 Å. This modification simplifies the analysis, because atoms on the diamond lattice do not interact with second neighbors who lie at a distance of 2.517 Å. The cutoff of 2.5 Å is applied only to the energy calculations in this analysis of the vacancy formation energy. Also we apply LCN to the analysis rather than TCN, since chemical concepts like the promotion energy require the total number of electrons on a given atom to be invariant as the atoms we brought together to form the bond. In Table I we give the cohesive energy and vacancy formation energy of carbon in the diamond structure calculated using the original TB and the reduced TB methods. The changes in the cohesive and vacancy formation energies introduced by the reduced TB simplifications are only 0.1% and 3%, respectively. Therefore, it is an excellent approximation to analyze the vacancy formation energy using the reduced TB method with LCN.

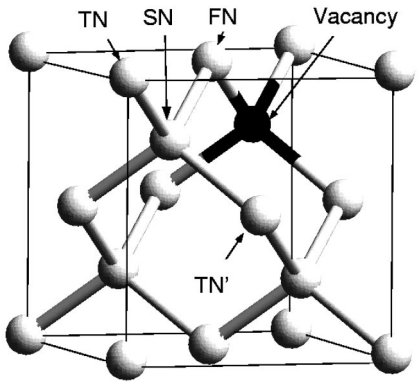

FIG. 8. Diamond lattice with a vacancy. FN and SN label the first- and second-neighboring atoms to the vacancy, respectively. Two kinds of third-neighboring atoms are distinguished by TN and TN′.

Figure 8 shows the diamond lattice with a vacancy. There are four first-neighboring (FN) and twelve second-neighboring (SN) atoms about the vacancy. The 24 third-neighboring atoms in total are grouped into two kinds of atoms (TN, TN′), each of them including 12 atoms. The number of valence s and p electrons and the corresponding promotion energy of the FN, SN, TN, and TN′ atoms are given in Table II. The number of valence s electrons on the FN atom increases by about 6% compared with that of a carbon atom in the perfect structure, which corresponds to an increase of 0.27 electrons in total over the four FN atoms. This increase in the number of s electrons on the FN sites reflects that the s component of the dangling bond is attracted firmly at the core of the carbon. The number of s electrons on the SN, TN, and TN′ atoms, on the other hand, is almost the same as that of the perfect structure. We see, therefore, from Table II that 97% of the total change in promotion energy resides in the FN shell of atoms about the vacancy, so that the redistribution of s and p valence electrons occurs mainly within the first shell. The change in the promotion energy stabilizes the vacancy by 1.858 eV.

Table III shows the bond orders and bond energies for σ

TABLE II. The number of valence s and p electrons and the promotion energies of the first- (FN), second- (SN), and third- (TN, TN′) neighboring carbon atoms about a vacancy in the diamond structure. $\Delta E_{\rm prom}$ is defined as the difference between the structure with a vacancy and the perfect structure in the promotion energy.

	Total	Perfect	FN	SN	TN	TN′	Others
N_s		1.203	1.271	1.203	1.202	1.205	
N_p		2.797	2.729	2.797	2.798	2.795	
$E_{\rm prom}$(eV/*atom*)		5.334	4.886	5.342	5.344	5.328	
$\Delta E_{\rm prom}$(eV/*atom*)			−0.448	0.008	0.010	−0.006	
Number of atoms	63		4	12	12	12	23
$\Delta E_{\rm prom}$(eV)	−1.858		−1.793	0.097	0.115	−0.076	−0.201
$\frac{\Delta E_{\rm prom}}{\Delta E_{\rm prom}({\rm Total})}\times 100(\%)$	100		96.5	−5.2	−6.2	4.1	10.8

TABLE III. The bond orders and the bond energies for σ and π bonds between the pairs of atoms FN-SN, SN-TN, and SN-TN′, respectively, in the presense of a vacancy. In the calculations of the bond energies E_σ and E_π, the hopping integrals are $h_\sigma = 9.903$ eV and $h_\pi = 1.533$ eV. ΔE_σ and ΔE_π are defined as the difference with the bond energy between the structure with a vacancy and the perfect structure. $\Delta E_{\sigma+\pi}$ represents $\Delta E_\sigma + \Delta E_\pi$.

	Total	Ideal	FN-SN	SN-TN	SN-TN′	Others
Θ_σ		0.9116	0.9161	0.9058	0.9107	
Θ_π		0.1036	0.1412	0.1034	0.1020	
E_σ(eV/bond)		−18.055	−18.143	−17.941	−18.036	
E_π(eV/bond)		−0.635	−0.866	−0.634	−0.625	
Number of bonds	124	124	12	12	24	76
E_σ(eV)	−2237.918	−2238.717	−217.718	−215.288	−432.866	−1372.046
E_π(eV)	−81.291	−78.740	−10.386	−7.605	−15.000	−48.300
$E_{\sigma+\pi}$(eV)	−2319.209	−2317.457	−228.105	−222.893	−447.866	−1420.362
ΔE_σ	0.799		−1.068	1.362	0.434	0.071
ΔE_π	−2.551		−2.766	0.015	0.240	−0.040
$\Delta E_{\sigma+\pi}$	−1.752		−3.835	1.377	0.674	−0.032
$\frac{\Delta E_\sigma}{\Delta E_{\sigma+\pi}(\text{total})} \times 100(\%)$	−45.6		61.0	−77.7	−24.8	−4.1
$\frac{\Delta E_\pi}{\Delta E_{\sigma+\pi}(\text{total})} \times 100(\%)$	145.6		157.9	−0.9	−13.7	2.3
$\frac{\Delta E_{\sigma+\pi}}{\Delta E_{\sigma+\pi}(\text{total})} \times 100(\%)$	100		218.9	−78.6	−38.5	1.8

and π bonds between the pairs of atoms FN-SN, SN-TN, and SN-TN′, respectively, in the presence of a vacancy. The σ bond order for FN-SN increases by 0.4%, whereas for SN-TN and SN-TN′ bonds it decreases by 0.6% and 0.1%, respectively, compared with that of the perfect structure. This oscillatory behavior in the variation of the bond orders reflects the screening of the vacancy. However, the very small variation in the σ bond order reflects the localized nature of the σ bonding in carbon, which is a strongly covalent material. For the π bonding the bond order between FN and SN atoms increases by 36% compared with that of the perfect structure. This increase means that the p electron of the dangling bond participates in the π bonding between FN and SN atoms rather than being attracted solely to the core of the carbon vacancy. If we had assumed that the bond orders are invariant to the formation of a vacancy, then the vacancy formation energy would have been overestimated by 1.752 eV. This additional stabilization energy to the formation of the vacancy is distributed between the σ and π bond energies, as −0.799- and 2.551-eV contributions, respectively. Thus, the absolute ratio of the σ to π contributions is about 1 to 3, which is considerably larger than the ratio of the σ and π bonding energy (18.054:0.635) in the perfect diamond lattice. In the σ bond energy the contribution of the SN-TN and SN-TN′ bonding to this stabilization energy is comparable to that of the FN-SN bonding. On the other hand, the stabilization energy for the π bonding comes from mainly the FN-SN bonding as the p electron in the dangling bond only participates in the π bonding between the FN and SN atoms. Finally, the total vacancy formation energy (9.783 eV) can be separated as the difference of the repulsive energy (−23.983 eV), the bond energy of the absent bonds reproduced by the vacancy (37.380 eV), the stabilization of the promotion energy (−1.858 eV), and the stabilization of the bond energy (−1.752 eV).

Figure 9 shows the errors in the bond orders for σ and π bonds between the FN and SN atoms. We see that the rate of convergence with respect to the number of recursion levels of the π bond order is twice as large as that of the σ bond order.

Thus, we have found that the block BOP can separate the different behavior of σ and π orbitals correctly. In particular, it can reproduce the different magnitude of reconstruction for the vacancy and the convergence rate with respect to the number of the recursion levels. In the scalar moment-based methods such as the scalar BOP method by Aoki and the global density of states (GDOS) method, the σ and π orbitals are not separated, since an averaged moment is used for the two kinds of orbitals.[9] This means that the different

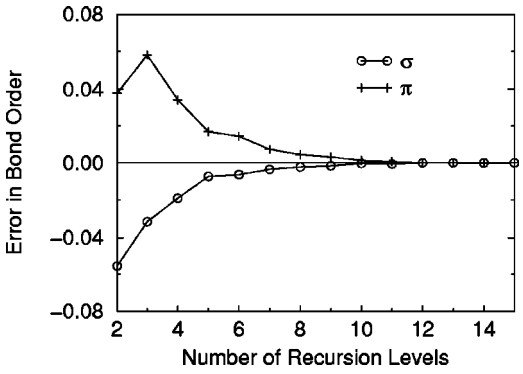

FIG. 9. The errors in the bond order for σ and π bonds between the FN and SN atoms, where the 15 recursion level bond orders $\Theta_\sigma = 0.9161$ and $\Theta_\pi = 0.1412$ were taken as the exact values.

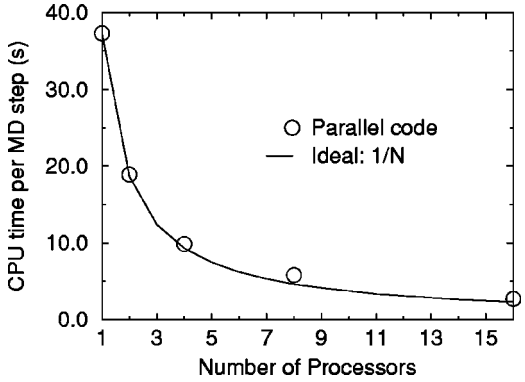

FIG. 10. The calculation time to evaluate the energy and the forces of a 512 atom carbon cell as a function of the number of processors by the parallel code. The benchmarks were performed on a Sun Ultra 10000 StarFire which is a parallel computer based on a shared-memory architecture, using a three-shell cluster, five recursion levels, and a square-root terminator.

properties of the *s* and *p* electrons in the dangling bond are averaged with respect to the vacancy formation energy and the convergence rate. As a result a great many moments are required in order to reproduce the vacancy formation energy in the usual scalar moment-based method.

V. LARGE-SCALE SIMULATION

The block BOP is applicable to the atomistic simulations of large systems including thousands of atoms. In this section we discuss the parallel computation required to perform such large-scale atomistic simulations and illustrate the method with an application to the deformation of a single-wall carbon nanotube under compression. It is very easy to give the program code with parallel structure because of the highly independent nature of the algorithm that evaluates the energy and force for each atom. We have only to structure essentially the three main loops in the program code in parallel: the block Lanczos transformation, the determination of the number of electrons on each atom, and the evaluation of forces. In these loops independent calculations can be performed for each atom, since no information needs to be passed between the individual atoms. The majority of the computational effort is occupied by the calculations in these three loops. Thus, if computation of the three loops are made parallel, we have almost the ideal parallel code. Figure 10 shows the time to evaluate the energies and forces of a diamond unit cell including 512 atoms as a function of the number of processors. It is found that the scaleability is almost ideal. The parallel computation was done using an automatic parallel compiler, which is able to perform an automatically restructuring of sequential code. The compiled code runs in parallel using the shared-memory multiprocessor machines. The ideal scaleability brought by the use of the automatic parallel compiler indicates the simplicity of the algorithms within block BOP.

We have performed a large-scale atomistic simulation for the deformation of a single-walled (10,10) nanotube under compression along the shaft as an application of the block BOP. The nanotube, which has a length of 140 Å, includes 2280 carbon atoms. The compression along the shaft was performed by the following geometric optimization with a constraint. First, the *z* coordinate of all the atoms in the nanotube oriented along the *z* axis are scaled as the length of shaft decreases 0.1% of its initial length. Second, the scaled structure is optimized geometrically with a constraint that the *z* coordinate of the atoms within 7 Å of both ends are kept fixed. By applying repeatedly the optimization to the nanotube, the shaft of the nanotube can be compressed statically. In the early stage of the compression the nanotube shrinks, maintaining the shape. However, the nanotube buckles periodically when the length of shaft reaches about 80% of the initial structure. Figure 11 shows a snapshot of the ripple-buckling nanotube. The mean wavelength of the ripple buckling is 4.8 Å. The appearance of the ripple buckling is very similar to the behavior observed by transmission electron microscope (TEM) and atomic force microscope (AFM) measurements.[47,48] A detail of discussion of the deformation and elastic properties of carbon nanotubes will be presented elsewhere.

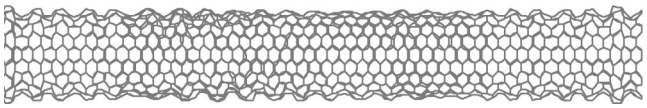

FIG. 11. Ripple-buckling single-wall (10,10) nanotube under compression along the shaft. The snapshot is at 80% of the initial length (140 Å). The calculation was performed with a five-hop logically truncated cluster, ten recursion levels, a square-root terminator, total charge neutrality, and $k_BT=0.1$ eV. Within the calculation conditions the error is about 1% in the bond energy for the initial structure compared with the *k*-space result.

VI. CONCLUSIONS

We have presented the theory of the block BOP based on the Lanczos basis representation and the block Lanczos algorithm with a single site as the starting state within the orthogonal tight-binding representation. The efficient O(N) algorithm provides a general recursion method for evaluating the bond energy and forces. In the Lanczos basis representation the off-diagonal block elements of Green's function matrix can be related to the diagonal block elements through a simple recurrence relation. As a result the bond orders can be easily evaluated. From the convergence properties for the bond energies and forces it is found that the method is applicable to a wide rage of materials (insulators, semiconductors, metals, and molecules) with a considerable reduction in the computational effort compared to *k*-space methods. The algorithm becomes more efficient than the *k*-space calculation when the number of atoms exceeds about 100. Constant-energy molecular dynamics simulations for carbon show that the forces are consistent with the total energy, even if the method is applied to liquids. Moreover, the use of the block Lanczos algorithm guarantees that block BOP represents the different properties of the σ and π bonds correctly, so that the vacancy formation energy of diamond is reproduced correctly with a small number of moments by a moments-based method. Finally, block BOP is very easy to set in parallel code; the parallel computation of the three main loops gives almost the ideal scaleability. The deformation of carbon nanotubes under compression was demonstrated as an appli-

cation of the method to large-scale atomistic simulations. Thus, we conclude that the block BOP is an efficient O(N) method to perform large-scale atomistic simulations of a wide variety of materials.

ACKNOWLEDGMENTS

We would like to thank A. P. Horsfield, I. I. Oleinik, D. Nguyen-Manh, and H. Nakamura for many useful discussions and many comments. T. O. gratefully acknowledges many encouragements and enlightening discussions with T. Mitani and Y. Iwasa. T. O. would like to thank the Department of Materials at Oxford University for their hospitality. M. A. and D. G. P. would like to thank the British Council for their support. Part of the computation in this work has been done using the computational facilities of the Material Modelling Laboratory (MML) in the Department of Materials at Oxford University.

APPENDIX

We derive a method for evaluating the exact force, which is consistent with the total energy, at any level of approximation. In this method the derivatives of the diagonal Green's functions can be evaluated indirectly by making use of the Lanczos basis representation, while the method is similar to the GDOS method[27] as regards the diagonal Green's functions are differentiated. The contribution from the band energy to the force is written using Eqs. (2) and (5) as follows:

$$\mathbf{F}_k^{(\mathrm{band})} = -\frac{\partial E_{\mathrm{band}}}{\partial \mathbf{r}_k} = \frac{2}{\pi}\mathrm{Im}\int \mathrm{tr}\left\{\frac{\partial G(E+\mathrm{i}0^+)}{\partial \mathbf{r}_k}\right\} E f(x)\,dE, \tag{A1}$$

The trace of the right side in Eq. (A1) can be divided into the diagonal block elements for individual atoms:

$$\begin{aligned}\mathrm{tr}\left\{\frac{\partial G(E+\mathrm{i}0^+)}{\partial \mathbf{r}_k}\right\} &= \sum_i \mathrm{tr}\left\{\frac{\partial \underline{G}_{ii}(E+\mathrm{i}0^+)}{\partial \mathbf{r}_k}\right\} \\ &= \sum_i \mathrm{tr}\left\{\frac{\partial \underline{G}_{00}^{L^{(i)}}(E+\mathrm{i}0^+)}{\partial \mathbf{r}_k}\right\},\end{aligned} \tag{A2}$$

where the index $L^{(i)}$ represents the representation based on the Lanczos basis with atom i as the starting site. In the Laczos basis representation the off-diagonal block elements of the Green's function matrix are evaluated through the recurrence relation Eq. (33), which is derived from the identity $(ZI-H)G(Z)=I$. Thus, the following useful relation can be derived for the derivative of the Green's function:

$$\frac{\partial G^{L^{(i)}}(Z)}{\partial \mathbf{r}_k} = G^{L^{(i)}}(Z)\frac{\partial H^{L^{(i)}}}{\partial \mathbf{r}_k} G^{L^{(i)}}(Z). \tag{A3}$$

Taking account of the (0,0) block element of both sides in Eq. (A3) we have

$$\mathrm{tr}\left\{\frac{\partial \underline{G}_{00}^{L^{(i)}}(Z)}{\partial \mathbf{r}_k}\right\} = \sum_{mn} \mathrm{tr}\left\{\underline{G}_{n0}^{L^{(i)}}(Z)\underline{G}_{0m}^{L^{(i)}}(Z)\frac{\partial \underline{H}_{mn}^{L^{(i)}}}{\partial \mathbf{r}_k}\right\}. \tag{A4}$$

Substituting Eqs. (A2) and (A4) for the trace in Eq. (A1) we can derive exactly the contribution from the band energy to the force at any level of approximation as the following very compact form:

$$\begin{aligned}\mathbf{F}_k^{(\mathrm{band})} &= -\sum_i \sum_{mn} \mathrm{tr}\left\{\underline{\tau}_{nm}^{L^{(i)}}\frac{\partial \underline{H}_{mn}^{L^{(i)}}}{\partial \mathbf{r}_k}\right\} \\ &= -\sum_i \sum_{m\alpha,n\beta} \tau_{n\beta,m\alpha}^{L^{(i)}}\frac{\partial H_{m\alpha,n\beta}^{L^{(i)}}}{\partial \mathbf{r}_k},\end{aligned} \tag{A5}$$

where

$$\underline{\tau}_{nm}^{L^{(i)}} = -\frac{2}{\pi}\mathrm{Im}\int E\underline{G}_{n0}^{L^{(i)}}(E+\mathrm{i}0^+)\underline{G}_{0m}^{L^{(i)}}(E+\mathrm{i}0^+)f(x)\,dE, \tag{A6}$$

where the summation for atom i is taken for all the atoms that include the atom k in the truncation of system. This expression for forces has a very similar form to the Hellmann-Feynman force [see Eq. (9)]. However, τ is a new dimensionless quantity indicating the strength of bonding between two Lanczos vectors.

A simple example is shown. Consider the force on atom 1 being at the end of a linear s-valent trimer along the x axis. It is assumed that the trimer has two electrons and the hopping integral between the pairs of atoms 1-2, 2-3, and 1-3 are $-h_1$, $-h_2$, and zero, respectively, where the h_1 and h_2 are positive and $h_2<h_1$, and also on-site energies for all the atoms are zero. If the recursion is approximated at the first levels, then the Green's functions are given as follows:

$$G_{00}^{L^{(1)}}(Z) = \frac{\frac{1}{2}}{Z-h_1} + \frac{\frac{1}{2}}{Z+h_1}, \tag{A7}$$

$$G_{01}^{L^{(1)}}(Z) = \frac{\frac{1}{2}}{Z-h_1} + \frac{-\frac{1}{2}}{Z+h_1}, \tag{A8}$$

$$G_{00}^{L^{(2)}}(Z) = \frac{\frac{1}{2}}{Z-\sqrt{h_1^2+h_2^2}} + \frac{\frac{1}{2}}{Z+\sqrt{h_1^2+h_2^2}}, \tag{A9}$$

$$G_{01}^{L^{(2)}}(Z) = \frac{\frac{1}{2}}{Z-\sqrt{h_1^2+h_2^2}} + \frac{-\frac{1}{2}}{Z+\sqrt{h_1^2+h_2^2}}, \tag{A10}$$

$$G_{00}^{L^{(3)}}(Z) = \frac{\frac{1}{2}}{Z-h_2} + \frac{\frac{1}{2}}{Z+h_2}, \tag{A11}$$

$$G_{01}^{L^{(3)}}(Z) = \frac{\frac{1}{2}}{Z-h_2} + \frac{-\frac{1}{2}}{Z+h_2}. \tag{A12}$$

The band energy of the trimer can be evaluated from the residues of the poles, which are occupied, in the diagonal elements of the Green's functions, namely,

$$E_{\text{band}} = -h_1 - \sqrt{h_1^2 + h_2^2}. \tag{A13}$$

In the force evaluation by Eq. (A5) we have only to calculate the $\tau_{01}^{L^{(1)}}$(or $\tau_{01}^{L^{(1)}}$), and $\tau_{01}^{L^{(2)}}$(or $\tau_{10}^{L^{(2)}}$), since the derivatives of Hamiltonian with respect to the position of atom 1 corresponding to other τ's are zero. The integrands for these τ's are

$$ZG_{00}^{L^{(1)}}(Z)G_{01}^{L^{(1)}}(Z) = \frac{\frac{1}{4}}{Z-h_1} + \frac{-\frac{1}{4}}{Z+h_1} + \frac{\frac{1}{4}h_1}{(Z-h_1)^2} + \frac{\frac{1}{4}h_1}{(Z+h_1)^2}, \tag{A14}$$

$$ZG_{00}^{L^{(2)}}(Z)G_{01}^{L^{(2)}}(Z) = \frac{\frac{1}{4}}{Z-\sqrt{h_1^2+h_2^2}} + \frac{-\frac{1}{4}}{Z+\sqrt{h_1^2+h_2^2}} + \frac{\frac{1}{4}\sqrt{h_1^2+h_2^2}}{(Z-\sqrt{h_1^2+h_2^2})^2} + \frac{\frac{1}{4}\sqrt{h_1^2+h_2^2}}{(Z+\sqrt{h_1^2+h_2^2})^2}. \tag{A15}$$

From the residues of the poles that are occupied we see that $\tau_{01}^{L^{(1)}}(=\tau_{10}^{L^{(1)}})$ and $\tau_{01}^{L^{(2)}}(=\tau_{01}^{L^{(2)}})$ are $-1/2$ and $-1/2$, respectively. Transforming the derivative of the Hamiltonian by Eq. (27) into the the Laczos basis representation we have

$$\frac{\partial H_{01}^{L^{(1)}}}{\partial x_1} = \frac{\partial H_{10}^{L^{(1)}}}{\partial x_1} = \frac{\partial h_1}{\partial x_1}, \tag{A16}$$

$$\frac{\partial H_{01}^{L^{(2)}}}{\partial x_1} = \frac{\partial H_{10}^{L^{(2)}}}{\partial x_1} = \frac{h_1}{\sqrt{h_1^2+h_2^2}}\frac{\partial h_1}{\partial x_1}. \tag{A17}$$

Thus, we can evaluate the contribution from the band energy to the force on atom 1 using Eq. (A5), namely,

$$\begin{aligned} F_{x_1}^{(\text{band})} &= -2\tau_{01}^{L^{(1)}}\frac{\partial H_{10}^{L^{(1)}}}{\partial x_1} - 2\tau_{01}^{L^{(2)}}\frac{\partial H_{10}^{L^{(2)}}}{\partial x_1} \\ &= -2\left(-\frac{1}{2}\right)\frac{\partial h_1}{\partial x_1} - 2\left(-\frac{1}{2}\right)\frac{h_1}{\sqrt{h_1^2+h_2^2}}\frac{\partial h_1}{\partial x_1} \\ &= \frac{\partial h_1}{\partial x_1} + \frac{h_1}{\sqrt{h_1^2+h_2^2}}\frac{\partial h_1}{\partial x_1}. \end{aligned} \tag{A18}$$

The result is identical to the contribution from the derivative of Eq. (A13) with respect to the x coordinate of atom 1. We see that the force by Eq. (A5) is certainly exact.

[1] M.K. Gilson, J.A. McCammon, and J.D. Madura, J. Comput. Chem. **16**, 1081 (1995).
[2] S.T. Wlodek, J. Antosiewicz, and J.A. McCammon, Protein Sci. **6**, 373 (1997).
[3] W. Kohn and L.J. Sham, Phys. Rev. **140**, A1133 (1965).
[4] O.F. Sankey and D.J. Niklewski, Phys. Rev. B **40**, 3979 (1989).
[5] A.P. Horsfield, Phys. Rev. B **56**, 6594 (1997).
[6] J.C. Slater and G.F. Koster, Phys. Rev. **94**, 1498 (1954).
[7] A.P. Sutton, M.W. Finnis, D.G. Pettifor, and Y. Ohta, J. Phys. C **21**, 35 (1988).
[8] D.G. Pettifor, Phys. Rev. Lett. **63**, 2480 (1989).
[9] M. Aoki, Phys. Rev. Lett. **71**, 3842 (1993).
[10] T. Ozaki, Phys. Rev. B **59**, 16 061 (1999).
[11] A.P. Horsfield, A.M. Bratkovsky, D.G. Pettifor, and M. Aoki, Phys. Rev. B **53**, 1656 (1996).
[12] A.P. Horsfield, A.M. Bratkovsky, M. Fearn, D.G. Pettifor, and M. Aoki, Phys. Rev. B **53**, 12 694 (1996).
[13] S. Goedecker and L. Colombo, Phys. Rev. Lett. **73**, 122 (1994).
[14] S. Goedecker and M. Teter, Phys. Rev. B **51**, 9455 (1995).
[15] W.T. Yang, Phys. Rev. Lett. **66**, 1438 (1991).
[16] G. Galli and M. Parrinello, Phys. Rev. Lett. **69**, 3547 (1992).
[17] F. Mauri, G. Galli, and R. Car, Phys. Rev. B **47**, 9973 (1993).
[18] F. Mauri and G. Galli, Phys. Rev. B **50**, 4316 (1994).
[19] X.-P. Li, R.W. Nunes, and D. Vanderbilt, Phys. Rev. B **47**, 10 891 (1993).
[20] M.S. Daw, Phys. Rev. B **47**, 10 895 (1993).
[21] G. Galli and F. Mauri, Phys. Rev. Lett. **73**, 3471 (1994).
[22] A. Canning, G. Galli, and J. Kim, Phys. Rev. Lett. **78**, 4442 (1997).
[23] S. Goedecker, Rev. Mod. Phys. **71**, 1085 (1999).
[24] D.R. Bowler, M. Aoki, C.M. Goringe, A.P. Horsfield, and D.G. Pettifor, Modell. Simul. Mater. Sci. Eng. **5**, 199 (1997).
[25] J.D. Kress and A.F. Voter, Phys. Rev. B **52**, 8766 (1995).
[26] A.F. Voter, J.D. Kress, and R.N. Silver, Phys. Rev. B **53**, 12 733 (1996).
[27] A.P. Horsfield, Mater. Sci. Eng., B **37**, 219 (1996).
[28] V. Heine, Solid State Phys. **35**, 1 (1980).
[29] D.G. Pettifor, *Bonding and Structure of Molecules and Solids* (Oxford University Press, Oxford, 1995).
[30] R. Haydock, V. Heine, and M.J. Kelly, J. Phys. C **5**, 2845 (1972); **8**, 2591 (1975).
[31] R. Haydock, Solid State Phys. **35**, 216 (1980).
[32] C. Lanczos, J. Res. Natl. Bur. Stand. **45**, 225 (1950).
[33] R. Jones and M.W. Lewis, Philos. Mag. B **49**, 95 (1984).
[34] J. Inoue and Y. Ohta, J. Phys. C **20**, 1947 (1987).
[35] D.C. Lay, *Linear Algebra and Its Applications* (Addison-Wesley, 1994).
[36] G. Golub and C.F. Van Loan, *Matrix Computations*, 3rd ed. (Johns Hopkins University Press, Baltimore, MD, 1996).
[37] D.M.C. Nicholson, G.M. Stocks, Y. Wang, and W.A. Shelton, Phys. Rev. B **50**, 14 686 (1994).
[38] C.H. Xu, C.Z. Wang, C.T. Chan, and K.M. Ho, J. Phys.: Condens. Matter **4**, 6047 (1992).

[39] L. Goodwin, A.J. Skinner, and D.G. Pettifor, Europhys. Lett. **9**, 701 (1989).
[40] A.P. Horsfield, P.D. Godwin, D.G. Pettifor, and A.P. Sutton, Phys. Rev. B **54**, 15 773 (1996).
[41] D.R. Bowler and M.J. Gillan, Comput. Phys. Commun. **120**, 95 (1999).
[42] A. Warshel and M. Karplus, J. Am. Chem. Soc. **94**, 5612 (1972).
[43] D.G. Pettifor, in *Many Atom Interactions in Solids*, edited by R. Nieminen, M.J. Puska, and M.J. Manninen, Springer Proceedings in Physics Vol. 48 (Springer-Verlag, Berlin, 1990), p. 64.
[44] D.G. Pettifor and I.I. Oleinik, Phys. Rev. B **59**, 8487 (1999).
[45] I.I. Oleinik and D.G. Pettifor, Phys. Rev. B **59**, 8500 (1999).
[46] D. Conrad and K. Scheerschmidt, Phys. Rev. B **58**, 4538 (1998).
[47] S. Iijima, Nature (London) **354**, 56 (1991).
[48] M.R. Falvo, G.J. Clary, R.M. Taylor II, V. Chi, F.P. Brooks, Jr., S. Washburn, and R. Superfine, Nature (London) **389**, 582 (1997).